Hindawi Publishing Corporation
Journal of Nanomaterials
Volume 2013, Article ID 587036, 6 pages
http://dx.doi.org/10.1155/2013/587036

Research Article

Broadband Near-Infrared Quantum Cutting in Metal-Ion Codoped $Y_3Al_5O_{12}$ Thin Films Grown by Pulsed-Laser Deposition for Solar Cell Application

Mei Kwan Lau and Jianhua Hao

Department of Applied Physics and Materials Research Centre, The Hong Kong Polytechnic University, Hung Hom, Kowloon, Hong Kong

Correspondence should be addressed to Jianhua Hao; apjhhao@polyu.edu.hk

Received 21 February 2013; Accepted 6 March 2013

Academic Editor: Feng Yan

We have deposited thin films of yttrium aluminum garnet (YAG) doped with Ce^{3+} and Yb^{3+} on quartz and silicon substrates by pulsed laser deposition. Near-infrared (NIR) quantum cutting which involves the emission of NIR photons through the downconversion from Ce^{3+} to Yb^{3+} is realized. Upon the broadband excitation of Ce^{3+} ions with a visible photon at the peak wavelength of 450 nm, NIR photons are generated by Yb^{3+} ions, with an emission wavelength centered at 1030 nm. The luminescent decay curves of Ce^{3+} were recorded as a supporting evidence corresponding to the energy transfer. This work offers a better and more convenient approach compatible with crystalline silicon solar cell compared to conventional bulk phosphors.

1. Introduction

Near-infrared (NIR) quantum cutting (QC) can be used to convert a photon with high energy into two photons of low energy to minimize the problem of thermalization of electron-hole pairs in a solar cell [1–3]. Attempt has been made to fully utilize the energy in the terrestrial solar spectrum in order to enhance the solar cell energy conversion efficiency [4]. The state-of-art commercial solar cells dominated in the market are based on crystalline silicon (c-Si). By considering the energy level structure of Yb^{3+} depicted in the Dieke diagram, Yb^{3+} ion can emit photons at around 1000 nm, which matches the energy gap of silicon (~1.1 eV) corresponding to the greatest spectral response [4]. Unfortunately, most reported NIR phosphors are still far from practical applications due to their narrow absorption bandwidth. Therefore, it is much necessary to find some novel pairs of donor and acceptor, which can efficiently convert broadband solar spectrum into NIR light matching the spectral response of silicon solar cells. Recently, the demonstration of broadband downconversion has attracted much attention [5–7]. On the other hand, so far, NIR QC phosphors are mainly limited to the form of powders or ceramics, which may not be feasible to the solar cell integration. The adverse light scattering of powder may limit its practical applications [8]. Meanwhile, the fabrication methods for those ceramic materials exhibiting NIR QC are less preferable due to the long reaction time and high temperature in solid-state processing [7]. In this work, we will report on the deposition of Ce^{3+}-Yb^{3+} codoped yttrium aluminum garnet ($Y_3Al_5O_{12}$; YAG) thin films showing broadband NIR QC characteristics, which offers a better and more convenient approach compatible with c-Si solar cell.

2. Experimental

YAG: Ce^{3+}, Yb^{3+} phosphors were fabricated by a sol-gel method using high purity Y_2O_3, Yb_2O_3, $Ce(NO_3)_3{\cdot}6H_2O$, $Al(NO_3)_3{\cdot}9H_2O$, citric acid, and polyethylene glycol as raw materials. The oxides were first dissolved in concentrated nitric acid and heated with continuous stirring. Deionized water was added when the solution became gel-like, then it was placed in an oven at 80°C until it had become completed dried. All reactants were thoroughly mixed with ethanol to obtain a transparent solution. The above solution was

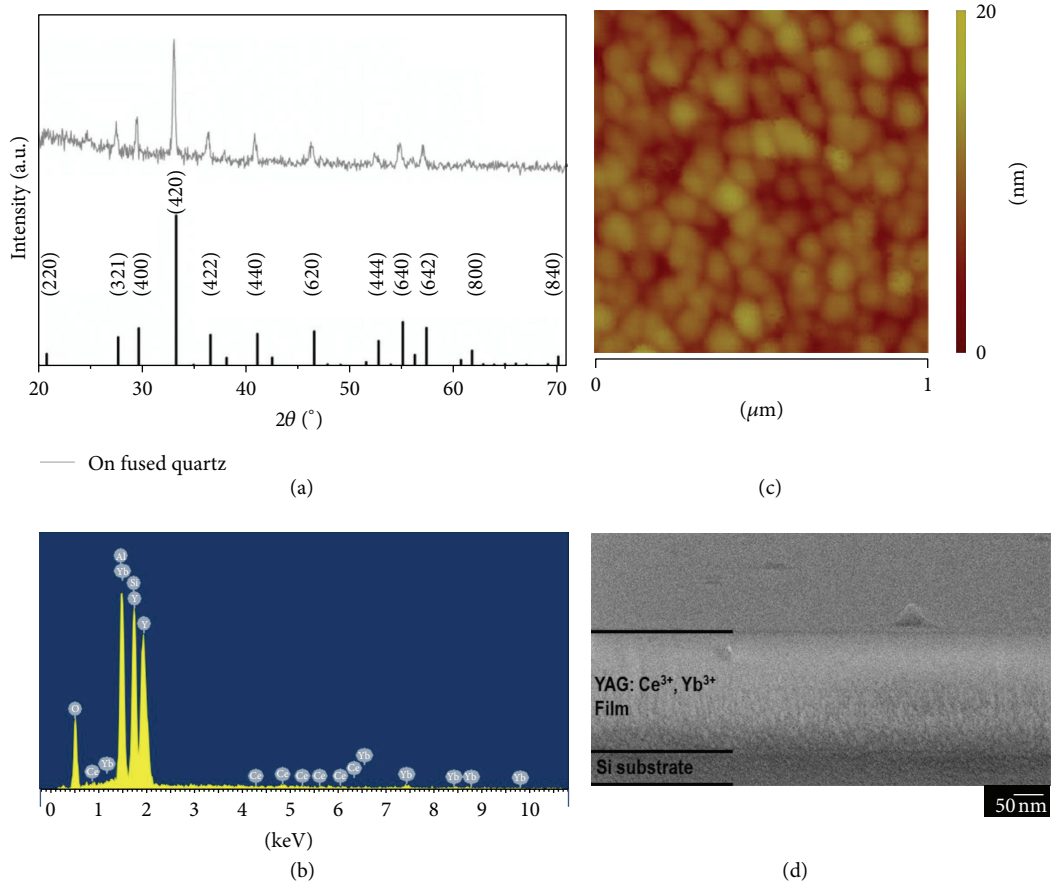

FIGURE 1: (a) XRD patterns of YAG: Ce^{3+}, Yb^{3+} thin film deposited on fused quartz, and the bars represent the diffraction pattern of the standard YAG phase. (b) EDX profile; (c) SPM image; (d) SEM image of YAG: Ce^{3+}, Yb^{3+} thin film deposited on silicon substrate.

kept in an oven at 80°C until it had been dried completely. The mixture was heated to 550°C for 4 h until a dark solid mass was formed. It was calcinated at 1000°C for 4 h after it had been grounded into powder form. Concentrations of the doping pairs were varied from 1 to 10 mol%. The mole ratio of 3 mol% Ce^{3+} to 5 mol% Yb^{3+} showed the highest photoluminescent response. The phosphor was mixed with polyvinyl acetates (PVAs) in a ratio of 10 g to 1.5 g and compressed to fabricate the target for pulsed laser deposition (PLD). The sintered target was ablated by focusing KrF excimer laser (λ = 248 nm) on the target. The cleaned fused silica and silicon (100) were used as the substrates. The chamber was pumped to a base pressure of 2×10^{-5} Torr prior to back filling with oxygen to obtain a partial pressure of 150 mTorr. The substrate temperature during deposition was kept at 600°C. After the deposition, the as-prepared film on fused quartz was further annealed at 900°C for 1 h in order to improve the crystallinity. The as-prepared films on Si were treated with rapid thermal processing (RTP) at 1000°C for 120 seconds. X-ray diffraction (XRD) was carried out to determine the crystal structure and identify the phase by the use of Bruker D8 Advance X-ray diffractometer. Energy dispersive X-ray spectroscopy was performed by using scanning electron microscope (SEM, JEOL Model: JSM-6490). The surface profile and roughness were obtained by the scanning probe microscope (SPM, Digital Instruments NanoScope IV). The optical spectroscopy was accomplished at room temperature through an FLSP920 fluorescence spectrometer from Edinburgh Analytical Instruments, which is equipped with a 450 W Xenon Lamp and a ns900 nanosecond flashlamp [9, 10].

3. Results and Discussion

Figure 1(a) illustrates the XRD profiles of the annealed thin film grown on fused quartz and the standard ICSD 04-1144. As indexed in the figure, all main diffraction peaks of the obtained film deposited on fused quartz agree well with the data for $Y_3Al_5O_{12}$. It indicates that the phase of YAG host is formed in the thin films and lanthanide ion doping has a little effect on the YAG phase formation. Meanwhile, the XRD profile of the film on silicon is dominated by the Si (400) peak (not shown here), suggesting that the film grown on Si is either amorphous or poorly crystallized. Figure 1(b) shows the EDX profile of the film grown on Si substrate; elements of the host material and doping ions are identified. Morphology of the films has been characterized using SPM and SEM. The morphology of the film grown on Si is consisted of small crystallites with the size of 50 nm on average, which is consistent to the structure measured by XRD. It is well

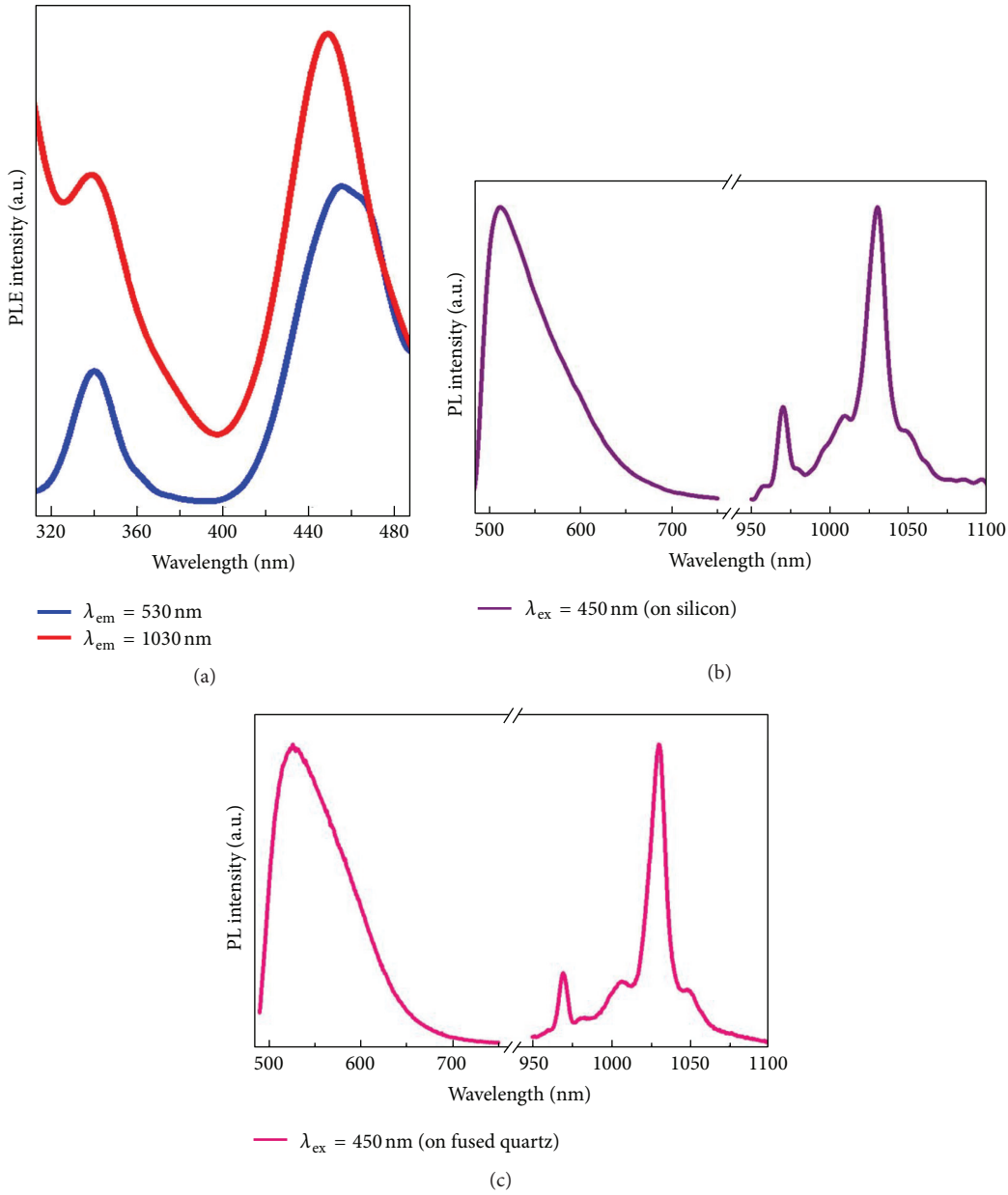

FIGURE 2: (a) PLE spectra of Ce^{3+} emission and the Yb^{3+} emission of YAG: Ce^{3+}, Yb^{3+} thin film. Normalized visible-NIR PL spectra of YAG: Ce^{3+}, Yb^{3+} thin film on (b) silicon wafer and (c) fused quartz.

known that the interdiffusion usually occurs between oxide and Si during PLD and postthermal treatment, which has a great effect on the crystallinity of oxide films grown on Si. More details will be studied with transmission electron microscopy and X-ray photoemission spectroscopy, similar to our previous study on oxide-based thin film [11, 12]. The surface roughness is about 20 nm, and the thickness is about 170 nm measured from the cross-sectional view of SEM. The film is highly transparent with transmittance over 84%.

The photoluminescence (PL) emission and excitation spectra of YAG: Ce^{3+}, Yb^{3+} are presented in Figure 2. In Figure 2(a), the excitation bands monitoring at 530 nm emission of Ce^{3+} and 1030 nm emission of Yb^{3+} are broad, where the peaks are centered at around 340 nm and 450 nm, respectively. This observation implies that the energy transfer from the $5d$ levels of Ce^{3+} to the $^2F_{5/2}$ level of Yb^{3+} is occurred upon the excitation with a visible photon. The excitation band located at 340 nm is attributed to the transition between $4f$ and $5d_2$ level of Ce^{3+}. Earlier study showed that [13] YAG singly doped with Pr^{3+} could exhibit downconversion. However, the reported excitation and emission are limited at discrete wavelengths; thus, the usefulness is reduced due to the narrow bands. Comparatively, the fabricated thin film that shows a broader excitation band ranging from 400 to 485 nm (FWHM ~ 40 nm) is presented in Figure 2, which is largely ascribed to the $4f$-$5d_1$ transition of Ce^{3+}. The obtained

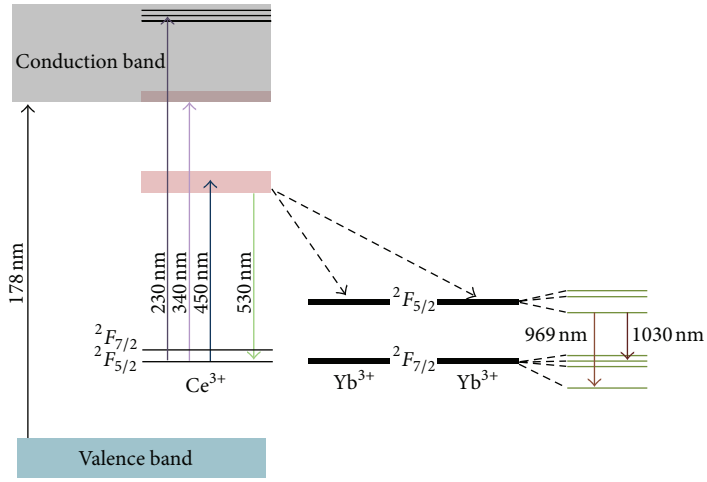

FIGURE 3: Schematic of energy level of Ce^{3+}/Yb^{3+} codoped YAG thin film and energy transfer mechanism of NIR QC under visible excitation at 450 nm.

results are also coincided with the previous work done by Liu et al. which indicated that Ce^{3+}-Yb^{3+} pairs may produce broader bandwidth in excitation compared with other Re^{3+}-Yb^{3+} (Re = Tb, Tm, and Pr) codoped materials [5].

The normalized PL spectra of the phosphor in both visible and NIR wavelength range by 450 nm excitation are plotted in Figures 2(b) and 2(c). It should be pointed out that the absolute PL intensity in different wavelength range cannot be compared since the emission spectra in the visible range and NIR range were recorded by different photomultipliers (PMTs). The emission band peaked at ~530 nm is ascribed to the transition of Ce^{3+} from $5d_1$ to $^2F_{5/2}$, while the emission located at 1030 nm is due to the $^2F_{5/2}$-$^2F_{7/2}$ transition of Yb^{3+}. Two weak shoulders on both sides of the characteristic NIR emission are assigned to the transitions among different stark levels of Yb^{3+} ($^2F_{5/2}$, $^2F_{7/2}$), as illustrated in Figure 3. The PL emission spectra of the films on both substrates show almost identical characteristics, including the emission peaks and bandwidth in the NIR range. It suggests that both of the two phosphor films with different crystalline form can play a role in converting high-energy photons in the solar spectrum to NIR photons. However, the PL intensity differs for the films grown on quartz and Si substrates under identical excitation condition, which could be ascribed to the different structure and interface of the films grown on different substrates as the above mentioned. It is worth to note that the emission in the NIR range cannot be observed in Yb^{3+} singly doped YAG samples excited by 450 nm, which further validates the hypothesis of the energy transfer from Ce^{3+} to Yb^{3+}.

The $4f$-$5d_1$ transition of Ce^{3+} is located at approximately twice the energy of the $^2F_{5/2}$-$^2F_{7/2}$ levels of Yb^{3+}, and there is no other level of Yb^{3+} up to the visible region. The energy transfer mechanism is proposed in Figure 3. The PL measurement results indicate that the emission of two NIR photons per absorbed visible photon with the Ce^{3+}-Yb^{3+} dual doping ions is mostly due to a cooperative energy transfer (CET). The broad excitation bandwidth of Ce^{3+} ions is particularly desirable in the view of photovoltaic application [7]. The mechanism responsible for the broadband excitation might be the allowed f-d transition and the excited electronic configuration of Ce^{3+} which has strong interaction with the neighboring anion ligands in the compounds [14]. Nevertheless, with the aid of strong crystal field strength of the YAG host material, the $5d$ level of Ce^{3+} is located in the visible range such that the high-energy photons in the solar spectrum are therefore converted to NIR photons from which silicon solar cell shows the greatest spectral response. A similar cooperative downconversion mechanism had been suggested for Ce^{3+}-Yb^{3+} codoped YBO_3 powder phosphor [14].

The dependence of the green and NIR PL intensity on Yb^{3+} concentration upon excitation at 450 nm is shown in Figure 4(a). With the increasing in Yb^{3+} concentration, the emission intensity in the visible range decreases monotonically, while the phenomena of concentration quenching are apparent for the NIR emission. To the certain extent, concentration quenching is due to the cross-relaxation between Yb^{3+} ions. To estimate the quantum efficiency (QE) of the phosphors, the decay curves of Ce^{3+} singly doped and Ce^{3+}-Yb^{3+} codoped YAG ablated targets were recorded and plotted in Figure 4(b) with the emission monitored at 530 nm under 450 nm excitation by a nanosecond flashlamp. The energy transfer efficiency (η_{ET}) is determined according to the following equation [15], which can deduce the theoretical maximum QE ($\eta_{x\%\,Yb}$) to be as high as 192%:

$$\eta_{ET} = 1 - \frac{\int I_{x\%\,Yb}\,dt}{\int I_{0\%\,Yb}\,dt},$$
$$\eta_{x\%\,Yb} = \eta_{Ce}\left(1 - \eta_{ET}\right) + 2\eta_{Yb}\eta_{ET}, \quad (1)$$

where I represents the luminescence intensity and x% Yb denotes the concentration in mol%. η_{Ce} and η_{Yb} are the quantum efficiency of Ce^{3+} and Yb^{3+}, respectively. Both of

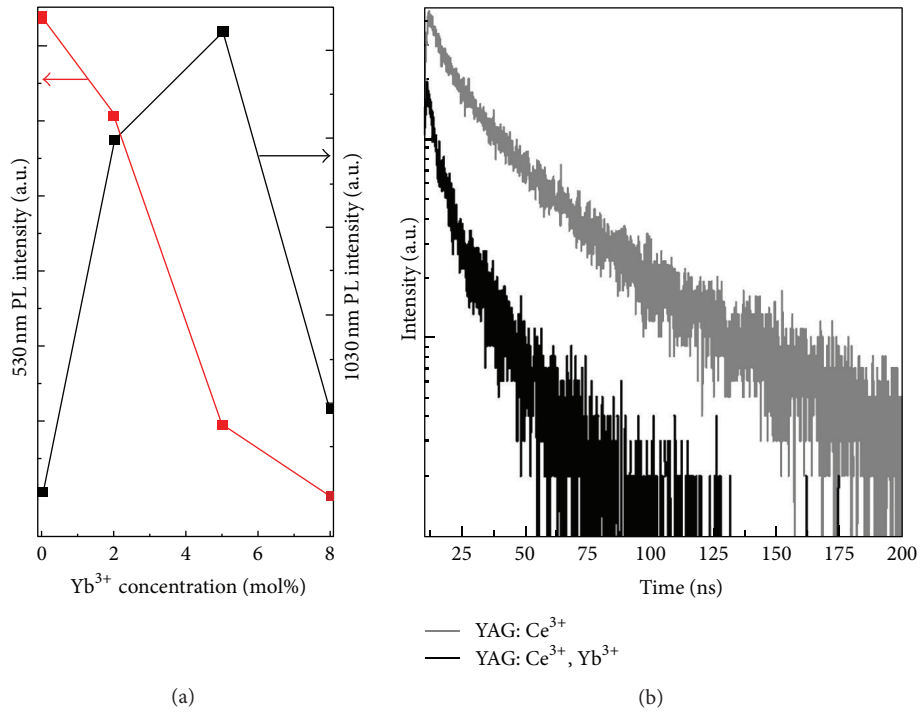

Figure 4: (a) PL intensity in the visible and NIR range as a function of Yb^{3+} concentration. (b) Decay curves of YAG: Ce^{3+}, Yb^{3+} under 450 nm excitation.

them are set to be unity [15]. Since the emission spectra in the visible range and NIR range were recorded by different PMT, the absolute quantum efficiency cannot be estimated from the relative NIR contribution. The effectiveness of thin-film emitters is determined by not only internal quantum efficiency but also light output coupling efficiency related to total internal reflection and the waveguide effect. Therefore, the overall effectiveness of thin-film emitters could be less than that of the corresponding bulks [16], including powder and ceramics. The present data do not permit a definitive answer whether the fabricated films are effective to enhance the efficiency of solar cell device. A more detailed study of the integrated system is required. At any rate, the results provided a broadband thin-film downconverter, offering a better and more convenient approach compatible with c-Si solar cell compared to powder or ceramic samples by considering the merits of thin film. Definitely, it is much needed to optimize the design and fabrication of the thin-film device to improve devices' efficiency in the future.

4. Conclusions

In conclusion, as a promising candidate to be integrated into silicon solar cell, Ce^{3+}-Yb^{3+} codoped YAG thin films on fused quartz and silicon wafers have been successfully achieved by PLD technique. XRD, SEM, and SPM analysis were performed to investigate the structural properties. NIR emission has been obtained through the energy transfer from Ce^{3+} to Yb^{3+}.

Acknowledgments

This work was supported by the Grants from the Research Grants Council of Hong Kong (GRF Project, no. PolyU5002/12P), the Hong Kong Polytechnic University Research Studentship (R-PAQ), and internal Grant (A-PK07).

References

[1] D. L. Dexter, "Possibility of luminescent quantum yields greater than unity," *Physical Review*, vol. 108, no. 3, pp. 630–633, 1957.

[2] C. Strumpel, M. McCann, G. Beaucarne et al., "Modifying the solar spectrum to enhance silicon solar cell efficiency: an overview of available materials," *Solar Energy Materials and Solar Cells*, vol. 91, no. 4, pp. 238–249, 2007.

[3] T. Trupke, M. A. Green, and P. Wurfel, "Improving solar cell efficiencies by down-conversion of high-energy photons," *Journal of Applied Physics*, vol. 92, no. 3, p. 1668, 2002.

[4] B. M. van der Ende, L. Aarts, and A. Meijerink, "Near-infrared quantum cutting for photovoltaics," *Advanced Materials*, vol. 21, no. 30, pp. 3073–3077, 2009.

[5] X. Liu, T. Yu, Y. Zhuang et al., "Broadband conversion of visible light to near-infrared emission by Ce^{3+}, Yb^{3+}-codoped yttrium aluminum garnet," *Optics Letters*, vol. 34, no. 22, pp. 3565–3567, 2009.

[6] S. Zhou, N. Jiang, B. Wu, J. Hao, and J. Qiu, "Ligand-driven wavelength-tunable and ultra-broadband infrared luminescence in single-ion-doped transparent hybrid materials," *Advanced Functional Materials*, vol. 19, no. 13, pp. 2081–2088, 2009.

[7] H. Lin, S. M. Zhou, and H. Teng, "Near infrared quantum cutting in heavy Yb doped $Ce_{0.03}Yb_{3x}Y_{(2.97-3x)}Al_5O_{12}$ transparent ceramics for crystalline silicon solar cells," *Journal of Applied Physics*, vol. 107, no. 4, Article ID 043107, 2010.

[8] D. Q. Chen, Y. S. Wang, Y. L. Yu, P. Huang, and F. Y. Weng, "Near-infrared quantum cutting in transparent nanostructured glass ceramics," *Optics Letters*, vol. 33, no. 16, pp. 1884–1886, 2008.

[9] Z. L. Wang, J. H. Hao, and H. L. W. Chan, "Down- and up-conversion photoluminescence, cathodoluminescence and paramagnetic properties of $NaGdF_4:Yb^{3+}$, Er^{3+} submicron disks assembled from primary nanocrystals," *Journal of Materials Chemistry*, vol. 20, no. 16, pp. 3178–3185, 2010.

[10] H. T. Wong, H. L. W. Chan, and J. H. Hao, "Magnetic and luminescent properties of multifunctional $GdF_3:Eu^{3+}$ nanoparticles," *Applied Physics Letters*, vol. 95, no. 2, Article ID 022512, 3 pages, 2009.

[11] J. H. Hao, J. Gao, Z. Wang, and D. P. Yu, "Interface structure and phase of epitaxial $SrTiO_3$(110) thin films grown directly on silicon," *Applied Physics Letters*, vol. 87, no. 12, Article ID 131908, 3 pages, 2005.

[12] J. S. Wu, C. L. Jia, K. Urban, J. H. Hao, and X. X. Xi, "Microstructure and misfit relaxation in $SrTiO_3/SrRuO_3$ bilayer films on $LaAlO_3$(100) substrates," *Journal of Materials Research*, vol. 16, no. 12, pp. 3443–3450, 2001.

[13] G. Özen, O. Forte, and B. Di Bartolo, "Downconversion and upconversion dynamics in Pr-doped $Y_3Al_5O_{12}$ crystals," *Journal of Applied Physics*, vol. 97, no. 1, Article ID 013510, pp. 013510–5, 2005.

[14] J. D. Chen, Hai Guo, Q. L. Zheng, and Y. X. Zhuang, "Near-infrared quantum cutting in Ce^{3+}, Yb^{3+} co-doped YBO_3 phosphors by cooperative energy transfer," *Optical Materials*, vol. 32, no. 9, pp. 998–1001, 2010.

[15] P. Vergeer, T. J. H. Vlugt, M. H. F. Kox, M. I. Den Hertog, J. P. J. M. Van Der Herden, and A. Meijerink, "Quantum cutting by cooperative energy transfer in $Yb_xY_{1-x}PO_4:Tb^{3+}$," *Physical Review B*, vol. 71, no. 1, Article ID 014119, 11 pages, 2005.

[16] S. Li, X. Zhang, Z. Hou, Z. Cheng, P. Ma, and J. Lin, "Enhanced emission of ultra-small-sized $LaF_3:RE^{3+}$ (RE = Eu, Tb) nanoparticles through 1, 2, 4, 5-benzenetetracarboxylic acid sensitization," *Nanoscale*, vol. 4, no. 18, pp. 5619–5626, 2012.